



Comparative Analysis of Electrode Materials for Alkaline Water Electrolysis

Performance Evaluation through Electrochemical Characterization

Lappeenranta–Lahti University of Technology LUT

Bachelor's Programme in Electrical Engineering, Bachelor's thesis

2026

Zhong Liu

Examiner(s): Junior Researcher Toni Viinanen

ABSTRACT

Lappeenranta–Lahti University of Technology LUT

LUT School of Energy Systems

Electrical Engineering

Zhong Liu

Comparative Analysis of Electrode Materials for Alkaline Water Electrolysis- Performance Evaluation through Electrochemical Characterization

Bachelor's thesis

2026

45 pages, 20 figures and 1 table

Examiner: Toni Viinanen

Keywords: Alkaline water electrolysis (AWE); nickel-based electrodes; electrochemical impedance spectroscopy (EIS); Tafel analysis; hydrogen evolution reaction (HER)

Alkaline water electrolysis is a mature and important green hydrogen production technology. But its efficiency is greatly affected by electrode materials. This thesis compares four nickel-based electrodes: pure nickel, nickel-plated stainless steel, foam nickel and Raney nickel, and focuses on their electrochemical properties in alkaline water electrolysis.

This study is based on experimental data obtained using a 30 wt.% KOH electrolyte at temperatures of 25 °C and 50 °C. The polarization behavior, resistance and dynamic parameters were evaluated by methods such as electrochemical impedance spectroscopy (EIS), IR correction and Tafel analysis. The results show that porous electrodes have better performance than dense electrodes due to their larger active surface area and better reaction kinetics. Raney nickel shows the best comprehensive performance, while nickel foam provides a more balanced option for practical application. By increasing the temperature from 25°C to 50°C, the performance of all materials has been improved, but the relative ranking remains unchanged.

Symbols and Abbreviations

Abbreviations

AWE	Alkaline Water Electrolysis
EIS	Electrochemical Impedance Spectroscopy
HER	Hydrogen Evolution Reaction
OER	Oxygen Evolution Reaction

Roman and Greek characters

E_{cell}	cell voltage	V
E_{rev}	reversible potential	V
E_{tn}	thermoneutral voltage	V
E_{measured}	measured cell voltage	V
$V_{\text{corrected}}$	IR-corrected voltage	V
I	current	A
j	current density	A/cm ²
j_0	exchange current density	A/cm ²
R_{Ω}	ohmic resistance	Ω
R_{ct}	charge transfer resistance	Ω
Z	impedance	Ω
b	Tafel slope	V/dec or mV/dec
F	Faraday constant	C/mol
R	gas constant	J/(mol·K)
T	temperature	K

p	pressure	Pa
$p_{\text{H}_2\text{O}}$	water vapour pressure	Pa
A	electrode area	cm^2
η	overpotential	V
α	charge transfer coefficient	–
ΔG	Gibbs free energy change	J/mol
ΔH	enthalpy change	J/mol
ΔS	entropy change	J/(mol·K)

Table of contents

1 Introduction	7
2 Theoretical Background	9
2.1 Thermodynamics of Water Electrolysis	9
2.2 Kinetics and Overpotential	10
2.3 Electrochemical Impedance Spectroscopy (EIS)	12
3 Methodology and Experimental Data	15
3.1 Materials and Electrolyte	16
3.2 Chronopotentiometry (I–V characterization)	17
3.3 Electrochemical impedance spectroscopy (EIS)	18
3.4 IR Correction	20
3.5 Tafel Analysis	21
4 Results and Discussion	23
4.1 Resistance results (from EIS experiments)	23
4.2 Polarization curves	25
4.2.1 Dense electrodes (Ni, NPSS)	25
4.2.2 Porous electrodes (Ni foam, Raney Ni)	29
4.2.3 Summary of polarization behavior	33
4.3 Tafel Plots and Comparison of Tafel Slopes	34
4.4 Exchange Current Densities and Charge Transfer Coefficients	36
4.5 Comprehensive Performance Comparison and Practical Implications	40
5 Conclusions	42
6 References	43

Tables and figures

DECLARATIONS

Turnitin

The originality of this thesis has been reviewed with the Turnitin similarity checking service.

AI usage

The author of this thesis, Zhong Liu, did not use any AI tools during the preparation of the thesis.

Responsibility

The author, Zhong Liu, takes full responsibility for the content of this thesis and has reviewed and edited the content generated by the possible use of AI tools.

1 Introduction

The transformation to a carbon-neutral energy system has positioned hydrogen energy as the core energy carrier of future power generation, energy storage and industrial processes. In particular, green hydrogen produced by water electrolysis driven by renewable electricity is considered to be a key driving factor for deep decarbonization in industries such as chemical manufacturing, steel production and long-term energy storage (IEA, 2019). Among the existing electrolysis technologies, alkaline water electrolysis (AWE) is still the most mature and industrially verified choice because of its robustness, scalability and relatively low system cost (Zeng and Zhang, 2010; Carmo et al., 2013).

In the AWE system, hydrogen and oxygen gas generation takes place through an electrochemical reaction at the cathode and anode surfaces, respectively. The electrolyte used in the system is a highly concentrated alkaline solution, usually in the form of potassium hydroxide or sodium hydroxide. While the AWE system's technology can be considered to be at an advanced level of maturity, the efficiency of the system's performance is still limited by voltage losses due to the following: the thermodynamic losses, the kinetics of the electrode's reactions, ohmic effects, and mass transfer effects (Santos et al., 2013). Of these effects, the electrochemical behavior of the materials used in the electrodes is the primary factor that controls the efficiency of the system's performance, especially under conditions of high current density (Schalenbach et al., 2018).

Ideal electrode materials for alkaline electrolysis must show high electrocatalytic activity to both hydrogen evolution reaction (HER) and oxygen evolution reaction (OER), while maintaining excellent corrosion resistance in a strong alkaline environment. Other requirements include good electrical conductivity, mechanical stability, and low material and manufacturing costs (Trasatti, 1991; McCrory et al., 2015). Nickel-based materials have become the most widely used non-precious metal electrodes for alkaline electrolysis because they have achieved a good balance between catalytic performance, durability and economic feasibility (Santos et al., 2013; O'Brien et al., 2005).

In addition to the material composition, the structure of the electrode has also been proven to have a key impact on the electrochemical properties. The porous three-dimensional structure can significantly increase the surface area of electrochemical activity, reduce the effective current density of the reaction site, and promote the separation of bubbles, thus reducing the activation and concentration overpotential (Carmo et al., 2013; McCrory et al., 2015). Raney nickel is prepared by selectively leaching aluminum from nickel aluminum alloy, which is an extreme case of microstructure optimization. Its excellent catalytic activity in alkaline hydrogen evolution reaction (HER) has long been recognized (Trasatti, 1991). Nickel foam also provides a support with high surface area and improved mass transfer properties, while dense materials such as pure nickel and nickel-plated stainless steel usually have high kinetic limitations.

This study directly compares and evaluates four representative nickel-based electrode materials: nickel-plated stainless steel, pure nickel, nickel foam and Raney nickel. Using chronopotentiometry and electrochemical impedance spectroscopy (EIS) data, the total voltage of the cell is decomposed into three contributions: thermodynamic, kinetic, and ohmic. Through mature electrochemical analysis methods, such as IR correction and Tafel fitting (Bard and Faulkner, 2001), key electrochemical parameters, including ohmic resistance, exchange current density and charge transfer coefficient, are extracted. In addition, the influence of working temperature is also investigated, because it affects the reaction kinetics and electrolyte conductivity in alkaline systems (Zeng and Zhang, 2010). The research results aim to provide quantitative guidance consistent with the literature for the selection and optimization of electrode materials in alkaline water electrolysis systems.

2 Theoretical Background

Alkaline water electrolysis is characterized by a complex interplay between thermodynamic limits, electrochemical kinetics, and resistive losses within the cell. A good understanding of all these aspects is necessary for proper interpretation of polarization curves and for separating material properties from system properties. Classically electrochemical theory is used to analyze current voltage curves, impedance diagrams, and kinetic parameters from experimental results.

2.1 Thermodynamics of Water Electrolysis

For standard conditions, water electrolysis is a non-spontaneous reaction with an endothermic heat of reaction. The necessary electrical input for spontaneous electrolysis is given by the change in Gibbs free energy, whereas the overall necessary electrical input is given by the enthalpy change for the reaction. These thermodynamic properties are used to define the cell voltage for spontaneous electrolysis and the thermoneutral voltage, from which the lower voltage limits for an electrolyzer are defined.

For an alkaline electrolyte, the reversible voltage for the hydrogen evolution reaction (HER) and oxygen evolution reaction (OER) is a function of temperature, hydroxide concentration, and gas pressures. These are given by the Nernst equation and are taken into account for calculations for 25 °C and 50 °C, where temperature-dependent reversible voltage is given for separating thermodynamic properties from voltage loss properties.

The minimum electrical energy required is defined by the change in Gibbs free energy, ΔG :

$$\Delta G = \Delta H - T\Delta S \quad (1)$$

where ΔG is the Gibbs free energy ($\text{J}\cdot\text{mol}^{-1}$), ΔH is the enthalpy change ($\text{J}\cdot\text{mol}^{-1}$), T is the temperature (K), ΔS is the entropy change ($\text{J}\cdot\text{mol}^{-1}\cdot\text{K}^{-1}$). The corresponding reversible cell voltage, E_{rev} , is derived from:

$$E_{rev} = \frac{\Delta G}{nF} \quad (2)$$

where $n = 2$ is the number of electrons transferred per molecule of H_2 produced, and F is Faraday's constant (96485 C/mol). At 25 °C and 1 bar, $E_{rev}=1.23V$. The thermoneutral voltage, $E_{tn} = \Delta H/nF \approx 1.48V$, represents the voltage at which the process is thermally balanced.

$$E_{tn} = \frac{\Delta H}{nF} \quad (3)$$

where E_{tn} is the thermoneutral potential (V).

$$E = E^\circ - \left(\frac{RT}{nF}\right) \ln Q \quad (4)$$

where E is the electrode potential (V), E° is the standard potential (V), R is the gas constant (8.314 J·mol⁻¹·K⁻¹), T is the temperature (K), and Q is the reaction quotient.

$$E_c = E_c^\circ - \left(\frac{RT}{2F}\right) \ln\left(\frac{1}{p_{H_2}}\right) \quad (5)$$

where E_c is the cathode potential (V) and p_{H_2} is the partial pressure of hydrogen (Pa).

$$E_a = E_a^\circ - \left(\frac{RT}{2F}\right) \ln(p_{O_2}) \quad (6)$$

where E_a is the anode potential (V) and p_{O_2} is the partial pressure of oxygen (Pa).

2.2 Kinetics and Overpotential

In practical electrolysis cells, it has been found that the measured cell voltage is always higher than the reversible potential due to kinetically limited interfaces between electrodes and electrolytes, as well as resistive losses in the system. The kinetics of current density vs. overpotential at an electrode interface can be described by the Butler-Volmer equation, in which forward and backward electrochemical reactions are in equilibrium.

At sufficiently high overpotentials, the Butler-Volmer equation can be reduced to the Tafel equation, allowing linear relationships between overpotential and logarithmic current density. This equation can be used to obtain critical parameters such as exchange current density and charge transfer coefficient, which can be used to quantify intrinsic

electrocatalytic activity. Tafel analysis is used in this study to obtain IR-corrected polarization curves.

The actual cell voltage, E_{cell} , exceeds E_{rev} due to various overpotentials (η):

$$E_{\text{cell}} = E_{\text{rev}} + \eta_a + \eta_c + I \cdot R_{\Omega} \quad (7)$$

where η_a and η_c are the total overpotentials at the anode and cathode (sum of activation and concentration overpotentials), and $\eta_{\text{ohm}} = I \cdot R_{\Omega}$ is the ohmic overpotential from resistances in the cell.

The current-overpotential relationship for a single electrode is described by the Butler-Volmer equation:

$$j = j_0 \left[e^{\frac{anF\eta}{RT}} - e^{-\frac{(1-a)nF\eta}{RT}} \right] \quad (8)$$

where j is current density, j_0 is the exchange current density (intrinsic activity), and α is the charge transfer coefficient (typically ~ 0.5), η is the overpotential (V), R is the gas constant, T is the temperature, and F is the Faraday constant.

At high overpotentials ($\eta > 50\text{mV}$), one exponential term dominates, simplifying to the Tafel equation:

$$\eta = a + b \log j \quad (9)$$

where η is the overpotential (V), b is the Tafel slope ($\text{V} \cdot \text{dec}^{-1}$), and a is a constant. Thus, j_0 and α can be extracted from experimental η vs. $\log(j)$ plots:

$$j_0 = 10^{-a/b} \quad (10)$$

$$b = 2.303 \frac{RT}{anF} \quad (11)$$

$$a = -b \cdot \log_{10}(j_0) \quad (12)$$

2.3 Electrochemical Impedance Spectroscopy (EIS)

Electrochemical impedance spectroscopy (EIS) is another electroanalytical technique that can be used to obtain additional information about electrolysis systems. This technique separates resistive and capacitive elements of the system over a range of frequencies. In an EIS diagram, the real axis intercept is related to ohmic resistance in the system, while semicircles are related to charge transfer at the interface.

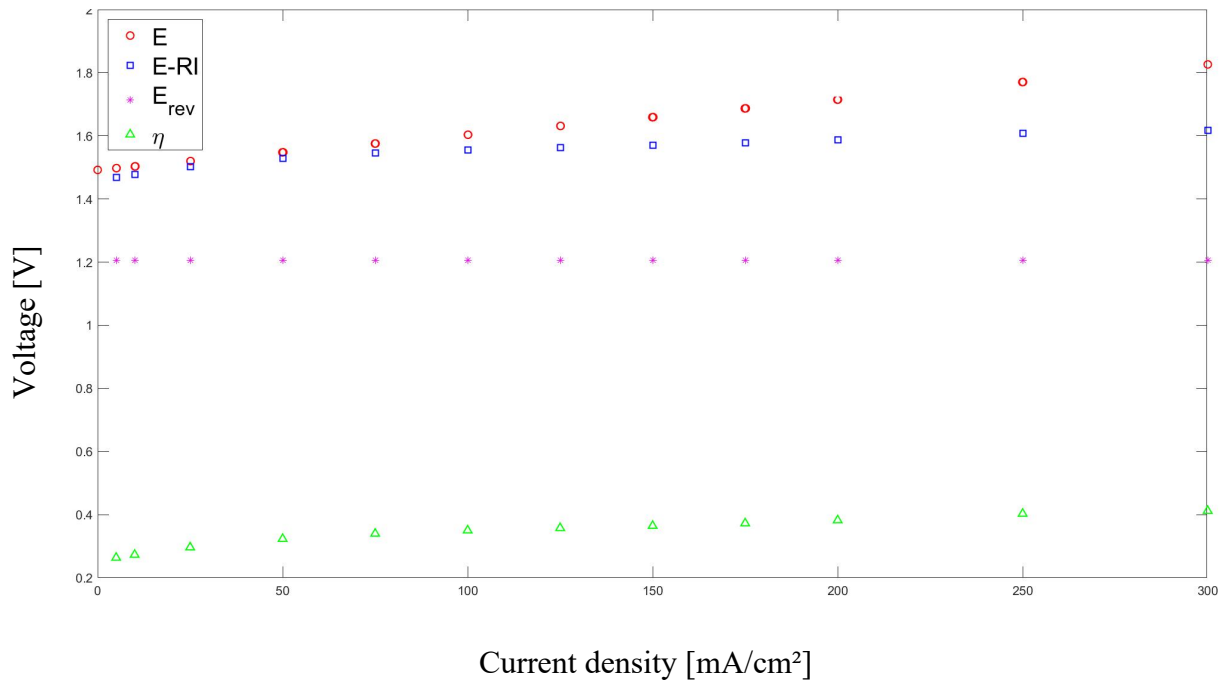


Figure 1. IR correction of polarization data.

EIS measures the cell's impedance as a function of frequency. A Nyquist plot (Imaginary vs. Real impedance) typically shows a high-frequency intercept on the real axis corresponding to the ohmic resistance (R_{ohm}), a semicircle related to the charge-transfer resistance (R_{ct}) in parallel with the double-layer capacitance, and possibly low-frequency features due to mass transport. R_{ct} is inversely related to j_0 .

In addition to the reversible voltage, the thermoneutral voltage represents the potential required for water electrolysis without pure heat exchange with the surrounding environment. It is defined in equation 3.

Although the electrochemical analysis conducted in this study does not directly use thermoneutral voltage, it provides an important reference for evaluating the energy efficiency of alkaline water electrolysis systems.

Under practical operating conditions, the partial pressures of hydrogen and oxygen deviate from their standard-state values due to the presence of water vapor. The effective partial pressures can be expressed as

$$p_{H_2} = p_c - p_{H_2O} \quad (13)$$

$$p_{O_2} = p_a - p_{H_2O} \quad (14)$$

p_c and p_a represent the total pressure of the cathode and anode respectively, and p_{H_2O} is the pressure of water vapor. Because the experimental device operates under conditions close to atmospheric pressure, these corrections are needed to accurately calculate the reversible electrode potential.

The temperature dependence of the water vapor pressure is estimated using the August–Roche–Magnus equation:

$$p_{H_2O} = 0.61094 e^{\frac{17.625T}{T+243.04}} \quad (15)$$

Where the vapor pressure is measured in kPa and the temperature is measured in °C. This expression is used to calculate the water vapor pressure at 25 °C and 50 °C, so as to ensure the consistency of gas pressure division and reversible potential determination.

From the linear fit of the Tafel plot, the exchange current density can be obtained from the intercept according to

$$j_0 = 10^{-\frac{a}{b}} \quad (16)$$

where j_0 is the exchange current density ($A \cdot cm^{-2}$), a is the intercept, and b is the Tafel slope. The exchange current density (j_0) represents the inherent electrocatalytic activity of the electrode material under equilibrium conditions.

The charge transfer coefficient can be determined from the Tafel slope using

$$\alpha = \frac{2.303RT}{bnF} \quad (17)$$

where α is the charge transfer coefficient. This parameter reflects the sensitivity of the electrochemical reaction rate to changes in overpotential and typically takes values between 0 and 1.

For kinetic analysis, the overpotential used in Tafel fitting is calculated as

$$\eta = E_{\text{measured}} - I \cdot R_{\Omega} - E_{\text{rev}} \quad (18)$$

Where E_{measured} is the voltage measured by the experiment, IR is the ohmic voltage drop measured by EIS, and E_{rev} is the reversible potential calculated according to the Nernst equation. This definition ensures that the extracted dynamic parameters are not affected by ohmic loss.

3 Methodology and Experimental Data

This study is based on a predefined set of experimental data obtained under controlled alkaline electrolysis conditions. Rather than generating new experimental results, the focus is placed on systematic analysis and interpretation of existing measurements, following standardized electrochemical characterization procedures provided by the supervisor.

Four nickel-based electrode materials are investigated: nickel-plated stainless steel, pure nickel, nickel foam, and Raney nickel. A 30 wt.% potassium hydroxide (KOH) aqueous solution is used as the electrolyte, representing typical industrial alkaline electrolysis conditions. All measurements are conducted at two temperatures, 25 °C and 50 °C, in order to evaluate the influence of temperature on thermodynamic, kinetic, and resistive contributions.

Constant-current polarization measurements are performed over a current density range of 5–300 mA/cm² using twelve discrete current steps. Each current point is maintained for five minutes to ensure steady-state conditions, and the sequence is applied in both ascending and descending order to minimize hysteresis effects. The entire sequence is repeated twice, improving measurement reliability and allowing consistency checks. Voltage signals are recorded using a potentiostat controlled via a customized LabVIEW program.

Electrochemical impedance spectroscopy measurements are conducted under zero direct current using EC-Lab software, covering a frequency range from 100 kHz to 100 mHz with a perturbation amplitude of 30 mA. To enable accurate separation of resistance contributions, impedance measurements are carried out separately for the anode, the cathode, and the full cell. The ohmic resistance is determined from the high-frequency intercept of Nyquist plots and subsequently used for IR correction of polarization data.

Data analysis follows a structured workflow. First, ohmic resistances are extracted from EIS measurements. Second, measured voltages are corrected for ohmic losses to obtain IR-free polarization curves. Third, reversible potentials are calculated at both temperatures using the Nernst equation. Finally, activation overpotentials are determined and used for

Tafel analysis to extract kinetic parameters. This integrated approach ensures internal consistency between different electrochemical characterization techniques.

3.1 Materials and Electrolyte

This study examined four electrode materials: nickel-plated stainless steel, pure nickel, nickel foam and Raney nickel. The electrolyte used is 30 wt.% solution of KOH.

Table 1. Current densities and corresponding absolute current values for the voltage measurements.

Current Density [mA/cm²]	Current [mA]
5	15,7
10	31,4
25	78,5
50	157
75	235,5
100	314
125	392,5
150	471
175	549,5
200	628
250	785
300	942

For the chronopotentiometry tests, constant current densities were used for the electrolysis cell. The current densities used range from low to relatively high current densities. The range of current densities ensures that the polarization curve for the electrodes is determined for the entire range of operating conditions. At each current density, the system is allowed to reach a stable voltage before the reading is taken.

The use of constant current densities for the chronopotentiometry tests ensures that the polarization curve for the electrodes can be determined. The polarization curve is essential for the comparison of the performance of different materials used for the electrodes. The

tests provide the basis for the subsequent analysis for the extraction of kinetic parameters and the correction for the IR drop.

Although chronopotentiometry supplies some information on the general polarization response of the cell, the various resistance contributions cannot be resolved with this method. Therefore, the electrochemical impedance spectroscopy technique has been used to investigate the ohmic and charge transfer resistance contributions to the system.

3.2 Chronopotentiometry (I–V characterization)

The current-voltage curve was measured at 25 °C and 50 °C. A total of 12 current density points were applied, ranging from 5 to 300 mA/cm². Each current step is maintained for 5 minutes, and the current loading order increases first and then decreases, and is repeated twice. The geometric area of the electrode is 3.14 cm². The voltage signal is recorded by a potentiostat controlled by a custom LabVIEW program (see Figure 2).

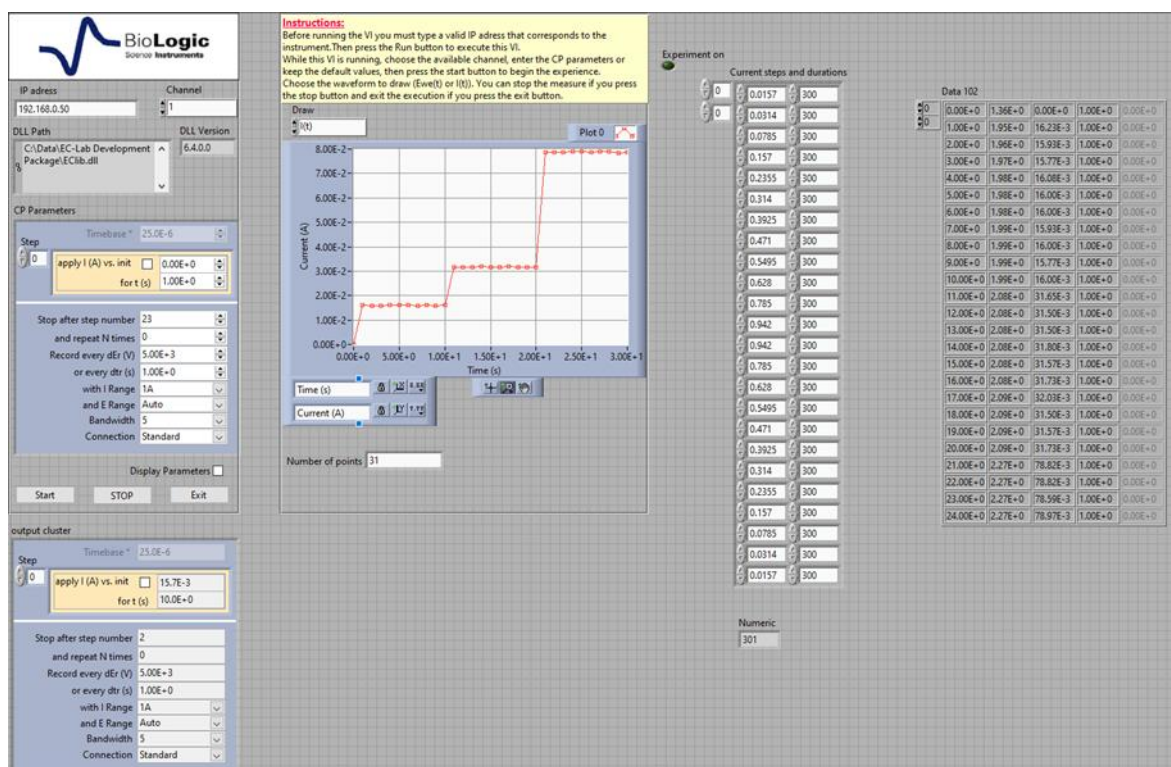


Figure 2. Chronopotentiometry driver in LabVIEW.

In chronopotentiometry, the voltages at the cell, the anode, and the cathode were recorded for all the current density steps. For each current density step, the voltages were stabilized,

after which a steady-state value was recorded from the plateau. For the reproducibility of the results, the experiment was repeated. As a result, the experiment provided two sets of data. For the cases where the experiment provided two sets of data, the results were compared to ensure reproducibility.

Besides impedance analysis, the parameters were also examined using Tafel analysis. This method enables the determination of the parameters of exchange current density and Tafel slope, which is helpful in understanding the kinetics of the reaction of the studied materials.

3.3 Electrochemical impedance spectroscopy (EIS)

The EIS test is carried out under zero direct current conditions, using a Biologic potentiostat and EC-Lab software. The test frequency range is 100 kHz to 100 mHz, and the AC perturbation amplitude is 30 mA. The anode alone, the cathode alone and the whole cell were measured respectively. The relevant parameters are shown in Figure 3. The intercept between the high-frequency end and the real axis in the Nyquist diagram (Figure 4) corresponds to the ohmic resistance R_{Ω} .

Excitation signal mode: Single sine

Set I_s = mA vs. <None>

for t_{I_s} = h mn s

Record every dE = mV

and dt = s

Scan from f_i = kHz

to f_f = mHz

with N_d = points per decade

in Logarithmic spacing

amplitude I_a = mA

wait for p_w = period before each frequency

average N_a = measure(s) per frequency

drift correction

Repeat n_c = time(s)

Limits

E Range = Resolution = *305,18 μ V*

I Range =

Bandwidth = (~ 1mn29s / scan)

Go back to seq. N_s = (*9999 ends technique*)

for n_r = time(s) (*0 for next sequence*)

increment cycle number

Figure 3. Parameters for EIS measurements in the EC-Lab software.

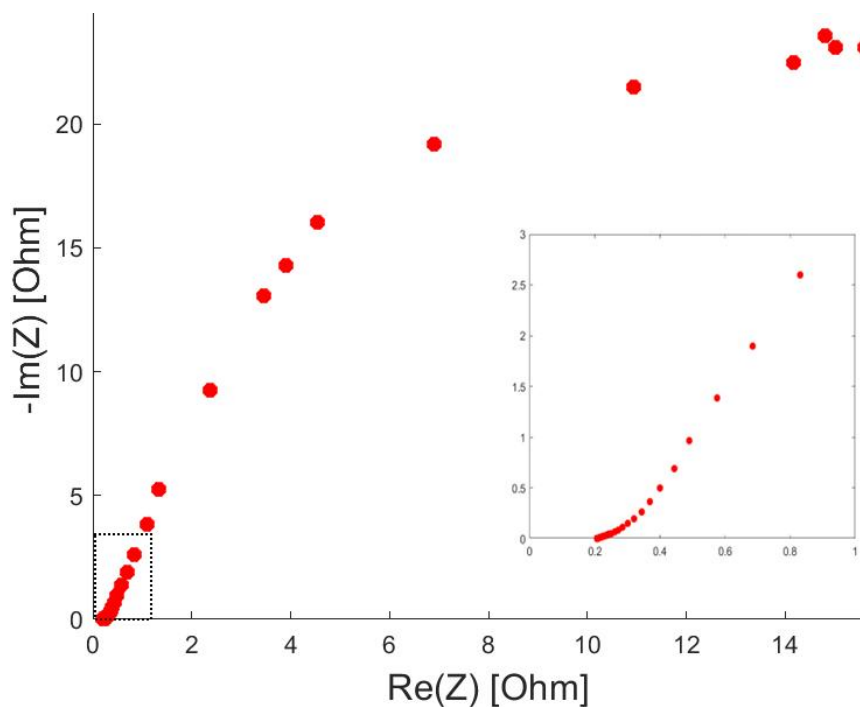


Figure 4. Example of a Nyquist plot from an electrode EIS measurement, with the real part of the impedance on the x-axis and the imaginary part on the y-axis.

The plot intersects the x-axis at high frequencies. A magnified view of the area marked at the bottom of the plot shows that the resistance R at the intersection point is approximately 0.2Ω .

Electrochemical impedance spectroscopy (EIS) was used to separate and quantify the different resistance contributions within the electrolysis cell. A Nyquist plot was obtained for the anode, cathode, and the entire cell at zero current. The ohmic resistance, R_{Ω} , was obtained from the intersection of the high-frequency end of the impedance diagram with the real axis. It mainly includes ionic resistance within the electrolyte, the resistance of the separator/diaphragm, contact resistances, and the cell geometry. These values of R_{Ω} were used to compensate the polarization curves for the IR drop.

3.4 IR Correction

The polarization curves obtained from the chronopotentiometry results contain information on both kinetic overpotential and ohmic losses in the electrochemical cell. The ohmic losses are mainly caused by the resistance of the electrolyte and separator materials, as well as electrical contacts and other materials in the electrochemical cell. In order to understand the electrochemical behavior of the materials used in the electrodes, correction of the voltage values was carried out based on the ohmic resistance.

The ohmic resistance of the electrochemical cell was obtained from electrochemical impedance spectroscopy results. The ohmic resistance is obtained from the intercept of the high-frequency impedance complex plane plot and the real axis of the plot. The ohmic resistance values were obtained from the impedance plot and were used in correcting the voltage values.

The IR correction of the voltage values was carried out using the following equation:

$$V_{\text{corrected}} = V_{\text{measured}} - I \times R_{\Omega} \quad (19)$$

Where V_{measured} is the experimentally measured cell voltage, I is the applied current, and R_{Ω} is the ohmic resistance obtained from the EIS measurements.

This correction allows the resistive losses to be separated from the total cell voltage. It also gives more accurate polarization data, which can be used in the kinetic analysis. The polarization curves, corrected using the IR correction, are then used in the next section for constructing Tafel plots and obtaining the kinetic parameters.

3.5 Tafel Analysis

Tafel analysis was carried out in order to determine the kinetic parameters of the electrode materials under investigation. This analysis was based on the polarization data, which was obtained from the chronopotentiometry curve. By analyzing the curve, where overpotential is plotted as a function of current density, kinetic parameters can be derived, which are very useful in understanding the electrochemical reaction.

The Tafel equation can be defined as:

$$\eta = a + b \log (j) \quad (20)$$

Here, η represents the overpotential, j represents the current density, and b represents the Tafel slope. By analyzing the linear region of the curve, the exchange current density j_0 and the Tafel slope can be derived. These parameters are very useful in understanding the kinetics of the electrode materials.

In order to perform the Tafel analysis, Tafel plots were constructed based on the polarization curve. Overpotential was calculated based on the reversible cell potential, ohmic drop, and cell voltage. By analyzing the curve, the linear region was identified, and linear regression was used in order to derive the Tafel slope and exchange current density.

An example of the Tafel plot used in this research is shown in Figure 5.

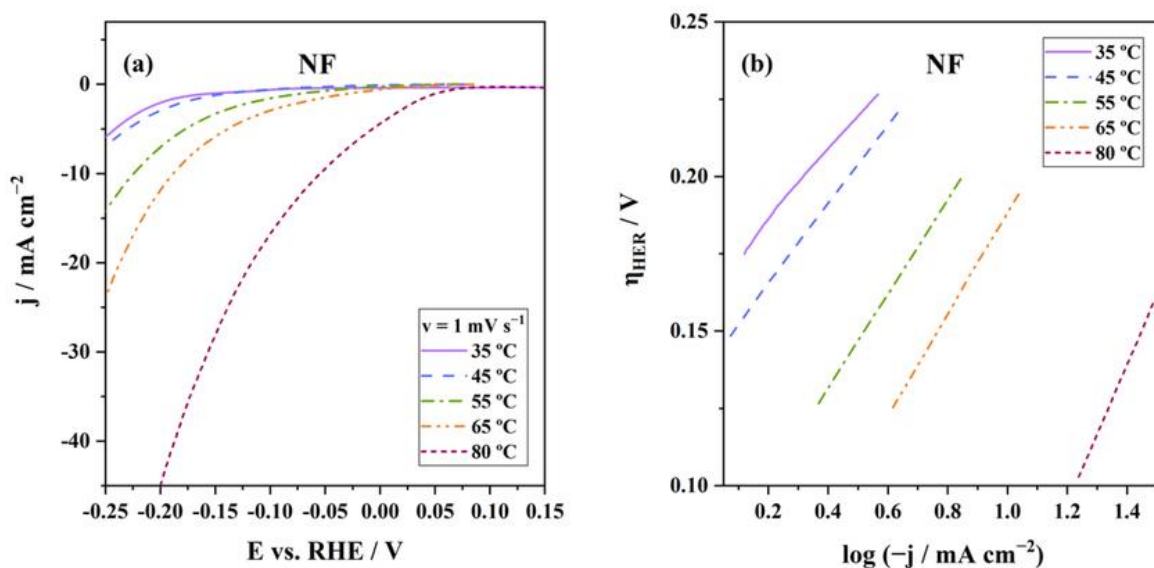


Figure 5. Tafel plots for the hydrogen evolution reaction (HER) on nickel foam electrode in alkaline water electrolysis at different temperatures. (Santos et al. 2023).

The parameters obtained from the Tafel analysis are of significant importance regarding the catalytic activity of the applied materials on the electrodes. The exchange current density is directly related to the reaction rate at equilibrium conditions, and the Tafel slope is related to how the reaction rate changes upon changes in the overpotential. By comparing these parameters for different electrodes, it is possible to assess how the structure of the electrodes affects the kinetics of the reaction during alkaline water electrolysis. The parameters are discussed in the next section together with polarization and impedance results.

4 Results and Discussion

Through a comprehensive analysis of polarization behavior, impedance characteristics and dynamic parameters, the electrochemical properties of the four electrode materials studied were evaluated. The results consistently show that the morphology and microstructure of electrodes play a crucial role in determining the alkaline electrolysis properties.

4.1 Resistance results (from EIS experiments)

In this section, the results of the resistance obtained from the EIS measurements for the studied materials are presented. The resistance of the anode, the cathode, and the full cell were obtained from the high-frequency intercept of the Nyquist plots, as shown in the bar graphs below.

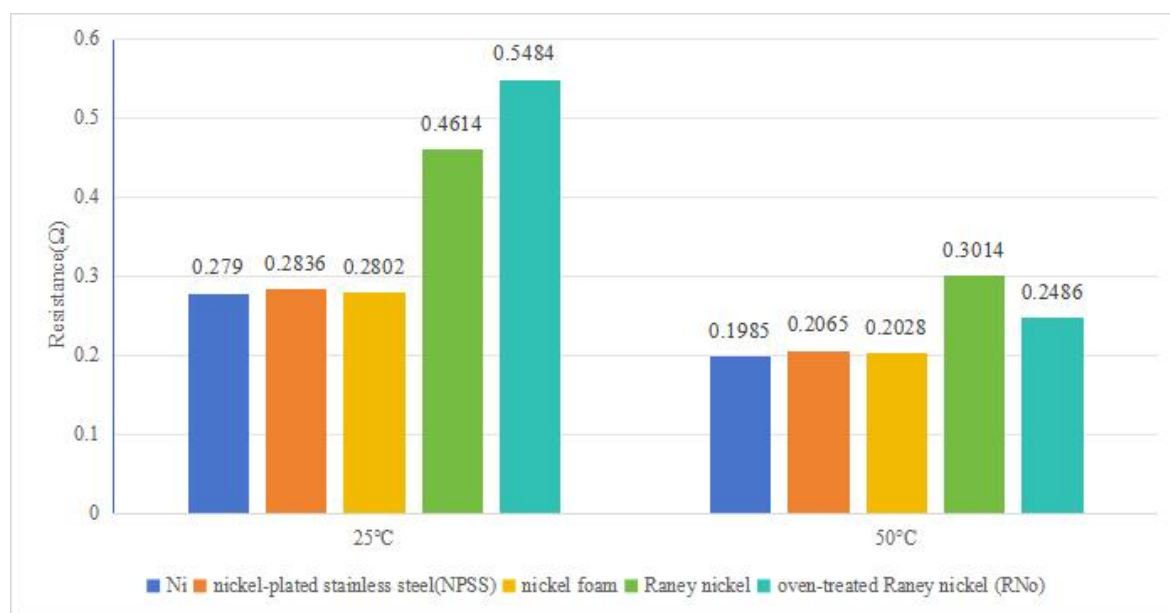


Figure 6. Anode-side resistance of different electrode materials.

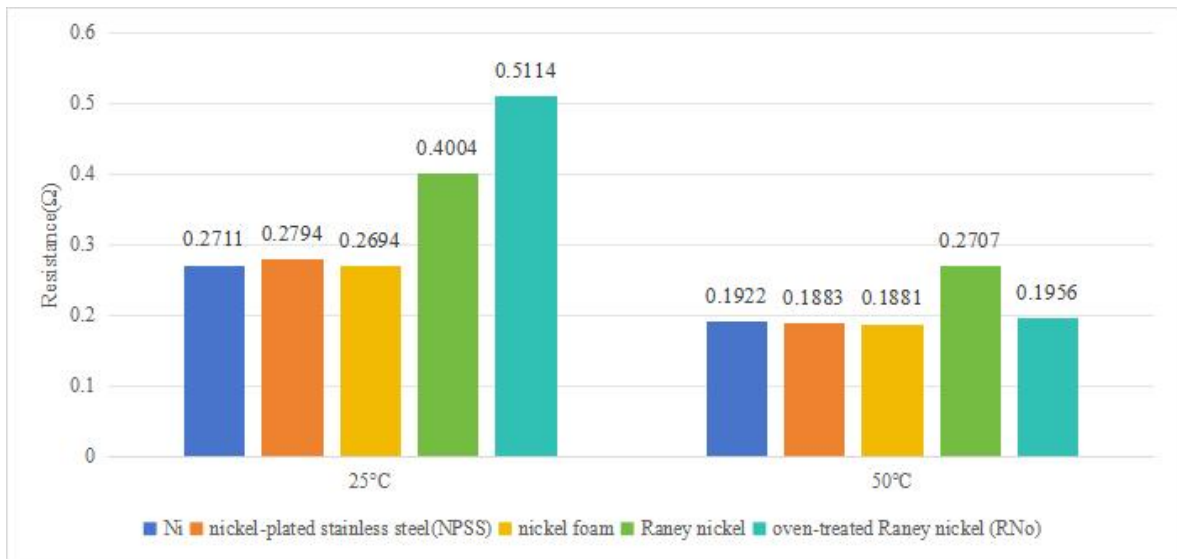


Figure 7. Cathode-side resistance of different electrode materials.

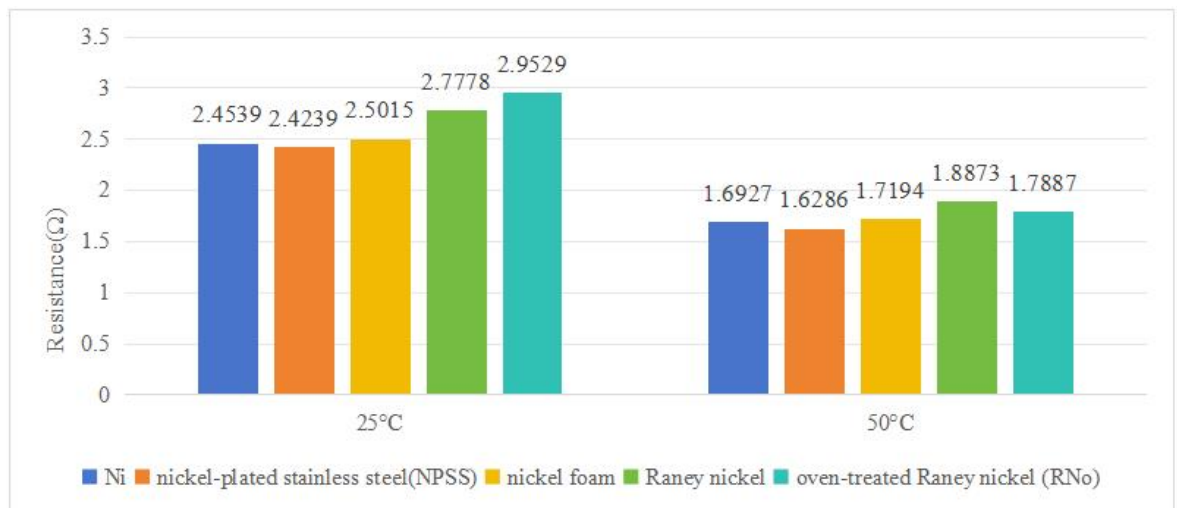


Figure 8. Total cell resistances.

The results show that the material used affects the resistance of the anode and the cathode of the cell. It can be seen that the electrode resistance of the materials, except for the Raney nickel, is relatively similar, while the Raney nickel shows the highest resistance among all the materials tested. However, the results show that the total resistance of the cell is less dependent on the materials tested, as the differences between the materials become less distinct.

This shows that the total resistance of the cell is not only dependent on the materials used but also on other factors, including the electrolyte, the separator, and the overall cell

configuration. It can also be seen from the results that the total resistance of the cell decreases as the temperature increases from 25 °C to 50 °C for all materials tested, which is consistent with the ionic conductivity of the electrolyte at a higher temperature.

4.2 Polarization curves

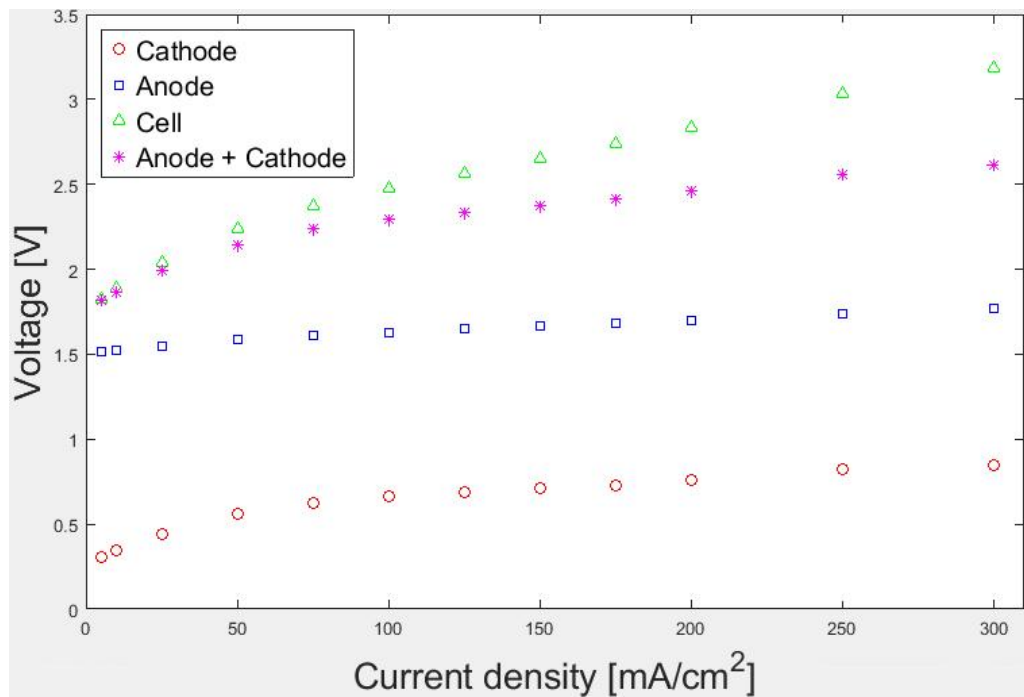
The polarization behavior of all investigated electrodes has been analyzed based on the chronopotentiometry test performed at 25 °C and 50 °C. Instead of describing the characteristics of all materials individually, the test results are presented for different types of electrode structure.

The cell voltage increases monotonically with the current density for all materials. This is due to the combined effect of activation, ohmic, and mass transport overpotentials. Increasing the temperature from 25 °C to 50 °C causes the cell voltage to decrease for the entire current density range. This suggests that the kinetics of the reaction and the conductivity of the electrolyte are enhanced. Moreover, the tests performed at the same conditions show similar results.

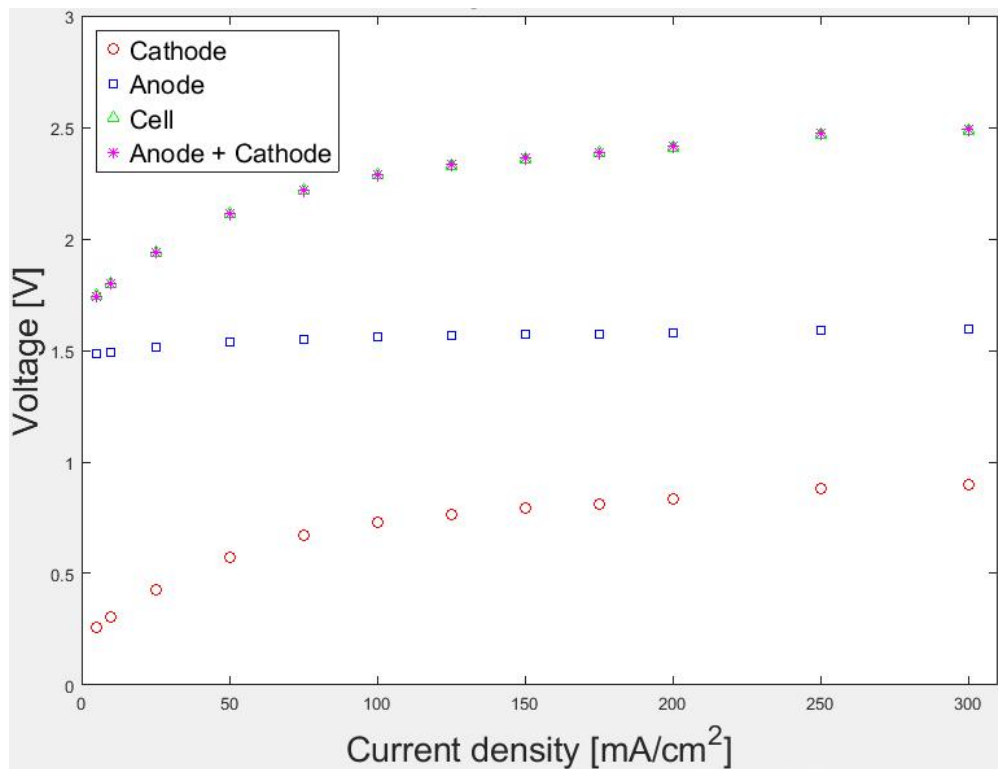
Based on the microstructure of the electrodes, they are classified as dense electrodes and porous electrodes.

4.2.1 Dense electrodes (Ni, NPSS)

Dense electrodes, like pure nickel and nickel-plated stainless steel, have relatively higher cell voltage compared to porous materials for all current densities.



(a) Nickel at 25 °C



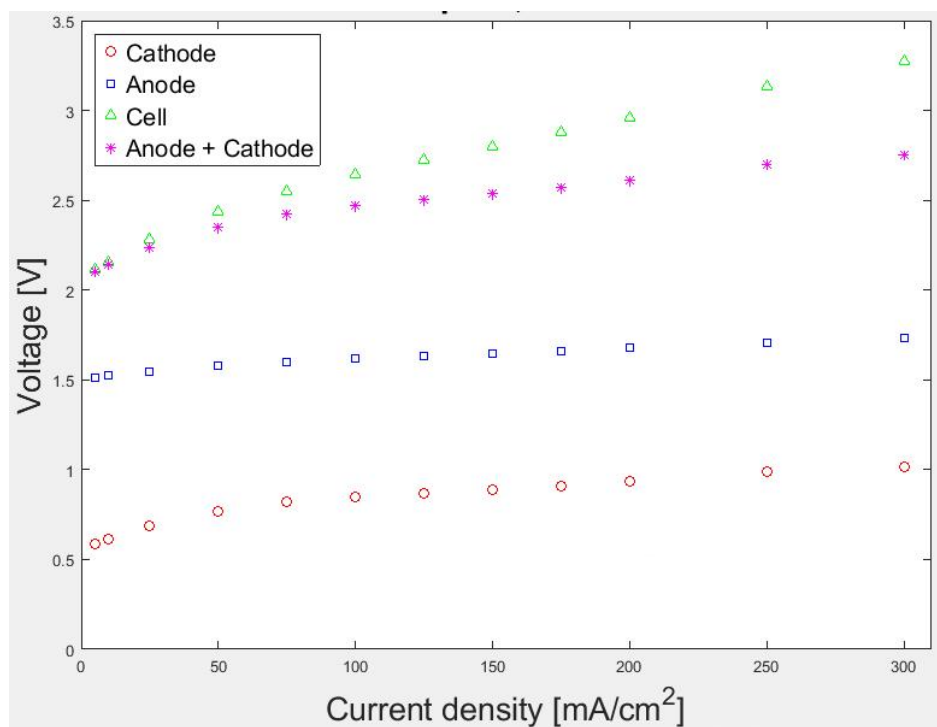
(b) Nickel at 50 °C

Figure 9. Chronopotentiometry polarization curves for pure nickel at 25 °C and 50 °C.

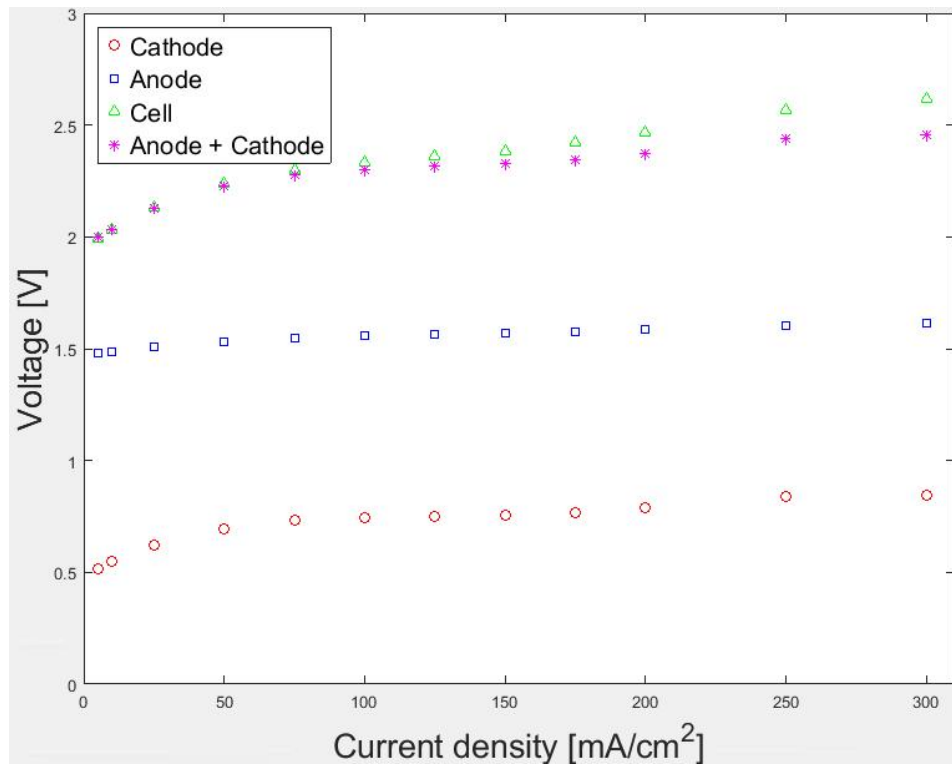
Two separate measurements were performed for each temperature to verify the data. The similarity between the measurements demonstrates good reproducibility of the data and stable electrode behavior. The lower voltage observed for the 50 °C case is an indication of improved kinetics and lower ohmic losses.

For both Ni and NPSS, the polarization curves show the expected increase in voltage with current density. The difference between the two materials is relatively small, showing that the electrochemical response of these materials is dominated by the limited active surface area and the relatively high charge transfer resistance.

Therefore, it can be concluded that the overall voltage reduction with increased temperature can be attributed to improved kinetics and reduced resistive losses. In addition, the dominant effect of increasing temperature is the improvement of reaction kinetics and electrolyte conductivity, which leads to lower activation and ohmic overpotentials. The change in reversible voltage with temperature is relatively small and has only a minor contribution to the total voltage reduction.



(a) NPSS 25 °C



(b) NPSS 50 °C

Figure 10. Chronopotentiometry polarization curves for nickel-plated stainless steel (NPSS) at 25 °C and 50 °C.

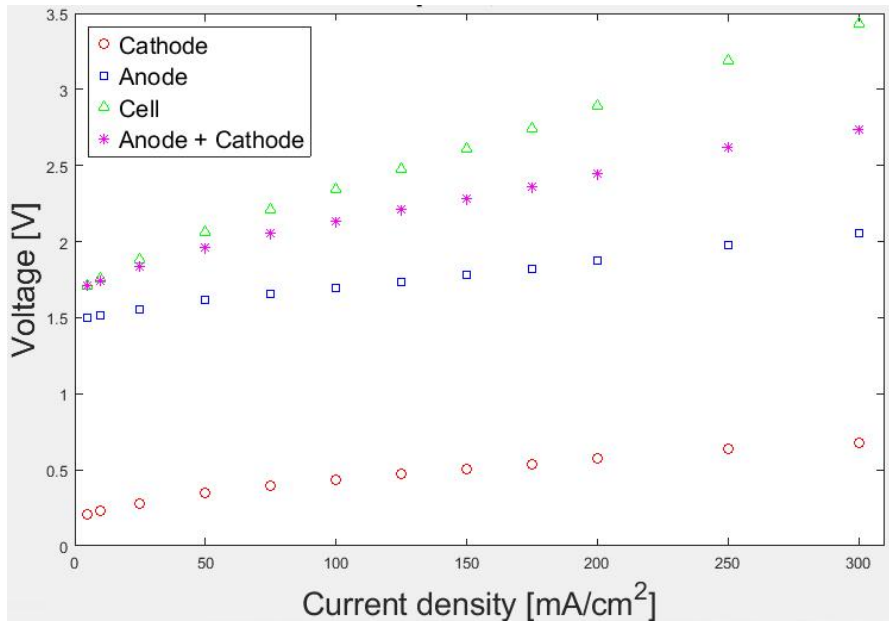
Two independent sets of measurements were conducted at both temperatures to evaluate the results. The voltage for the cathode, anode, and the complete cell are displayed as a function of the current density. The decrease in the cell voltage with the increase in temperature shows that the kinetics are improved.

When the temperature is increased to 50 °C, there is a noticeable voltage reduction over the entire range of current density. This is mostly due to improved reaction kinetics and reduced ohmic resistance.

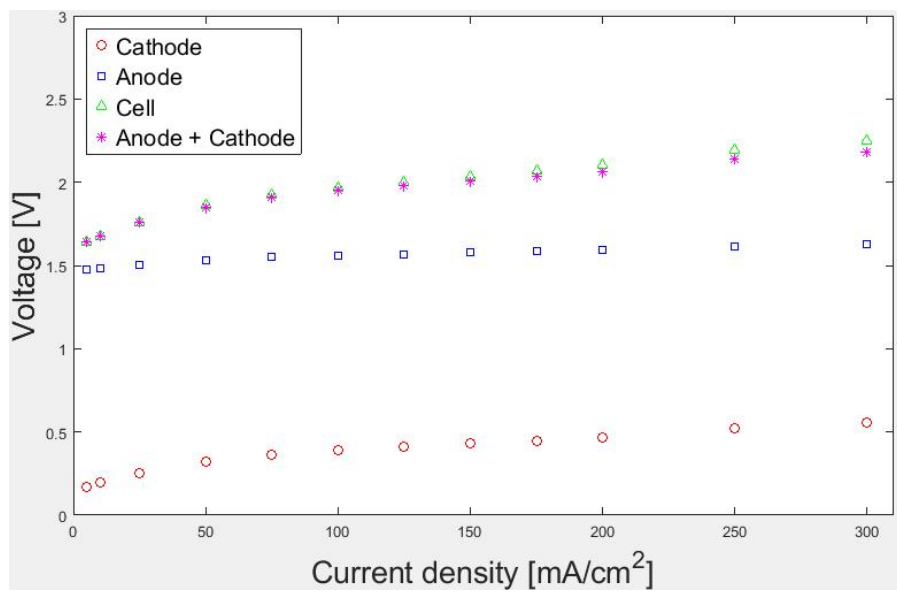
Therefore, dense electrodes have a limited performance due to their low electrochemically active surface area, thus increasing the activation overpotential compared to porous structures.

4.2.2 Porous electrodes (Ni foam, Raney Ni)

Porous electrodes such as nickel foam and Raney nickel electrodes, both hydrogen-treated and oven-treated, have been shown to have much better electrochemical properties compared to dense electrodes.



(a) Ni-foam 25 °C

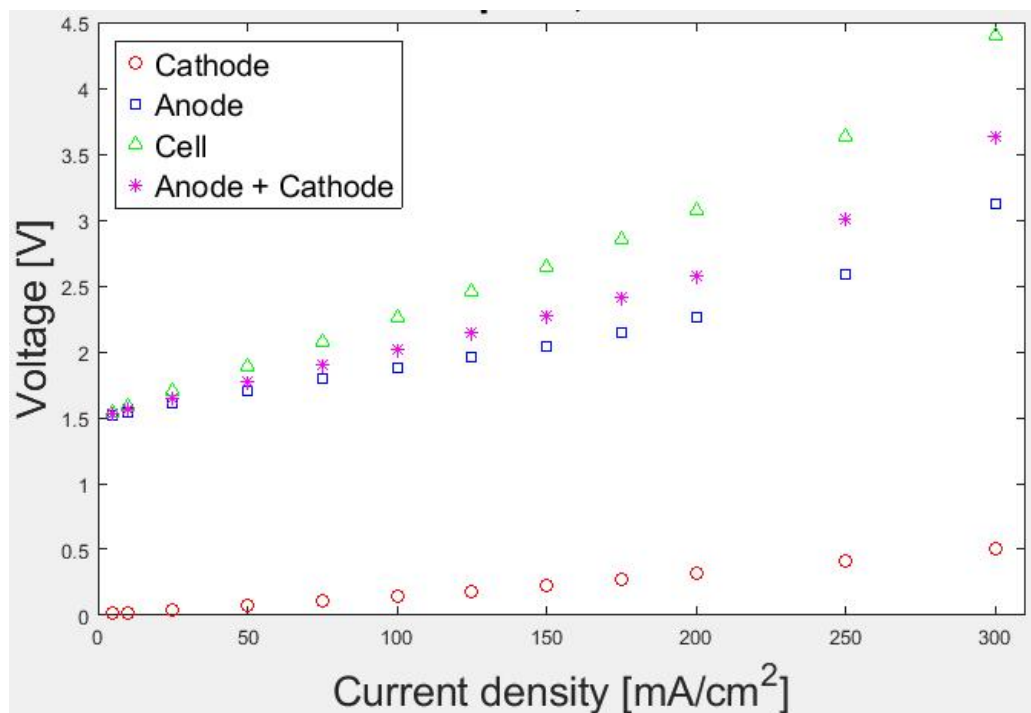


(b) Ni-foam 50 °C

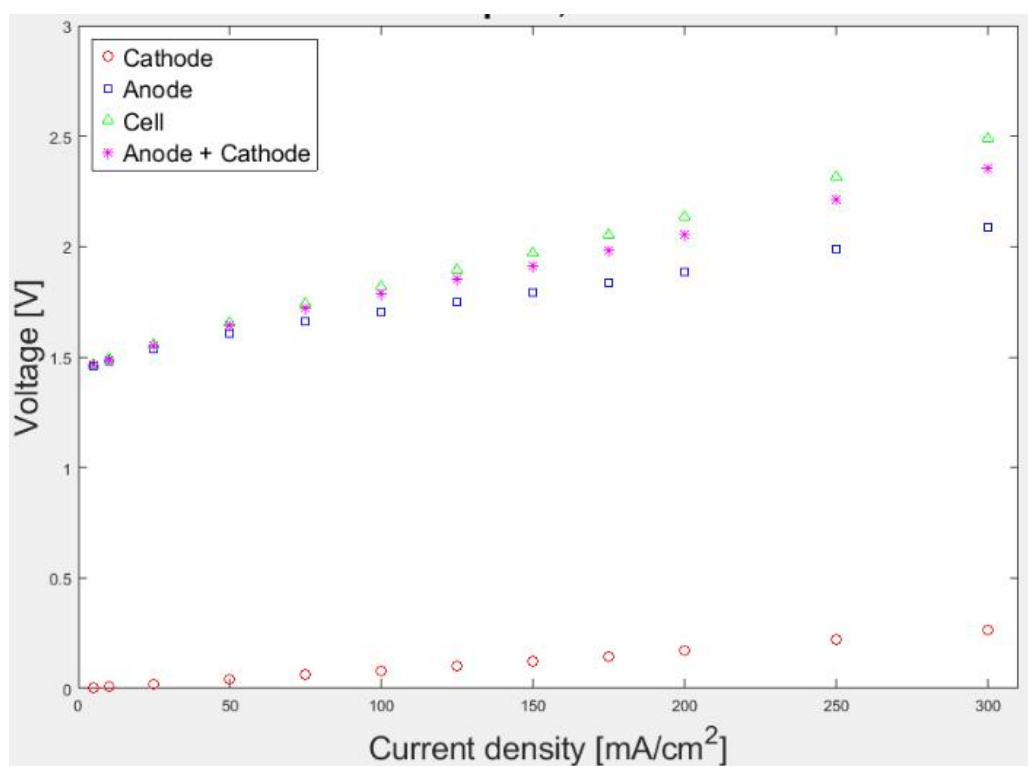
Figure 11. Chronopotentiometry polarization curves for nickel foam measured at 25 °C and 50 °C.

For each temperature, two independent measurements were performed to verify the data. As expected, the similarity between the measurements confirms the stable behavior of the electrodes, while the lower voltage observed at 50 °C is a consequence of the improved kinetics and lower ohmic drop.

At all these temperatures, the materials show lower cell voltages for the entire current density range. This is because of the materials' three-dimensional porous structure, which increases the electrochemically active surface area.

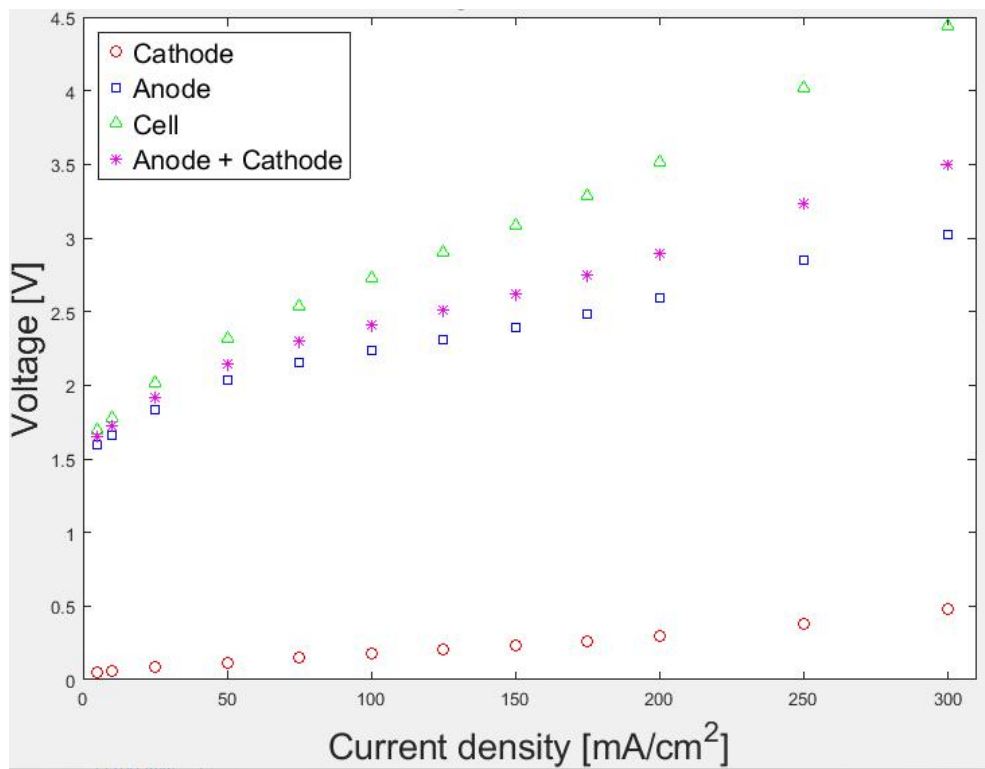


(a) RN (H₂)25 °C

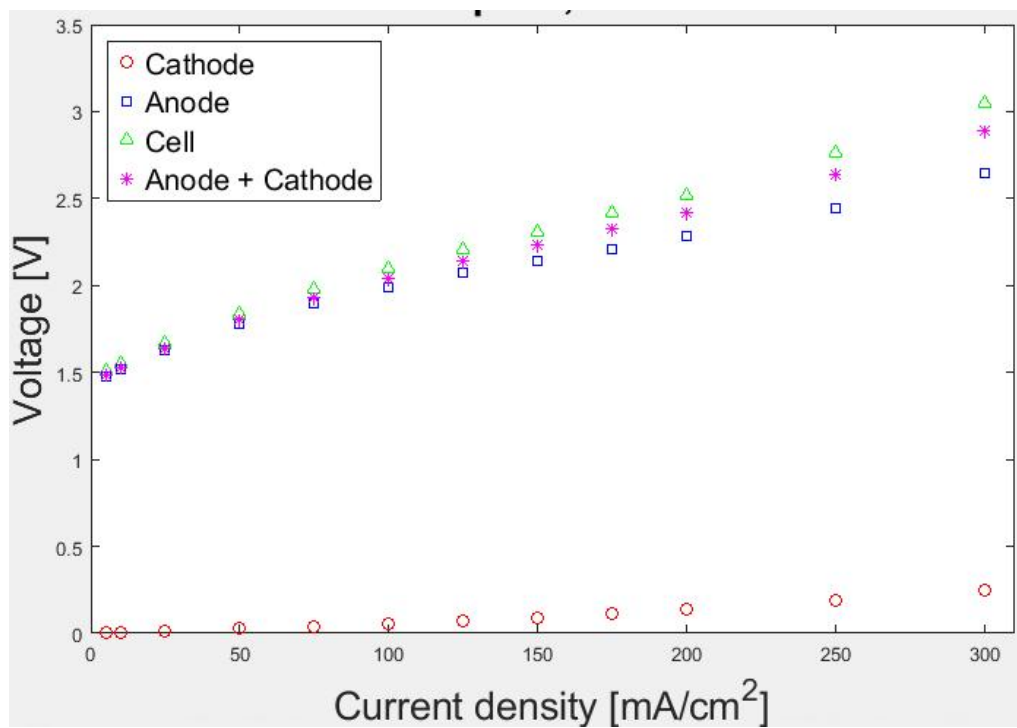


(b) RN(H₂) 50 °C

Figure 12. Chronopotentiometry polarization curves for hydrogen pre-treated Raney nickel at 25 °C and 50 °C.



(a) Raney(oven) 25 °C



(b) Raney(oven) 50 °C

Figure 13. Chronopotentiometry polarization curves for oven-treated Raney nickel at 25 °C and 50 °C.

It can be noted that the method of pretreating the Raney nickel has a lesser impact on the performance of the electrode compared to the effect of increasing the temperature.

Among the porous materials, Raney nickel displays the lowest overpotential, thus the highest catalytic activity. The performance of hydrogen-treated and oven-treated Raney nickel is only slightly different, with hydrogen treatment yielding a better performance at lower current densities owing to better surface activation.

Similar to dense electrodes, an increase in temperature to 50 °C results in a decrease in voltage for all porous materials. However, the relative performance of the materials is unchanged, suggesting that the effects of temperature on the performance of the materials are similar.

The results also show that the performance of the electrodes is highly reproducible, as evidenced by the high correlation of the results with repeated measurements.

The better performance of the porous electrodes is attributed primarily to the minimization of charge transfer resistance and improvement of kinetics, which is more dominant in the determination of cell voltage.

4.2.3 Summary of polarization behavior

From this comparison between dense and porous electrodes, it is obvious that microstructure is a factor of critical importance in electrochemical performance.

- Porous electrodes (Ni foam, Raney Ni): lower cell voltage due to kinetics enhancement and enlarged active surface area
- Dense electrodes (Ni, NPSS): limited by high activation overpotential
- Temperature increase improves performance of all materials, though ranking remains unchanged

These trends provide the basis for further analysis using EIS and Tafel methods in the following sections.

4.3 Tafel Plots and Comparison of Tafel Slopes

Tafel analysis was performed using IR-corrected polarization curves to examine the reaction kinetics of the tested electrode materials. An example of a logarithmic Tafel plot is first presented to describe the linear fitting procedure for determining the kinetic parameters. Based on this linear region, the Tafel slope for each tested material is determined and compared in figures 15 and 16.

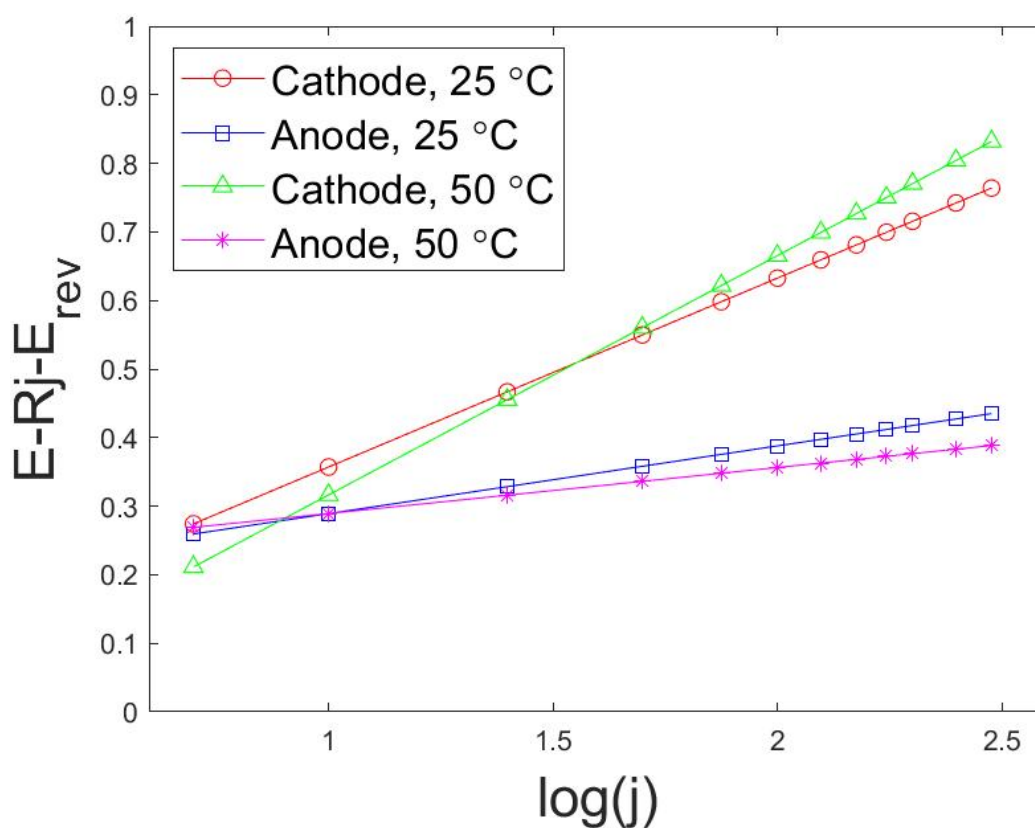


Figure 14. Example Tafel plots for pure nickel

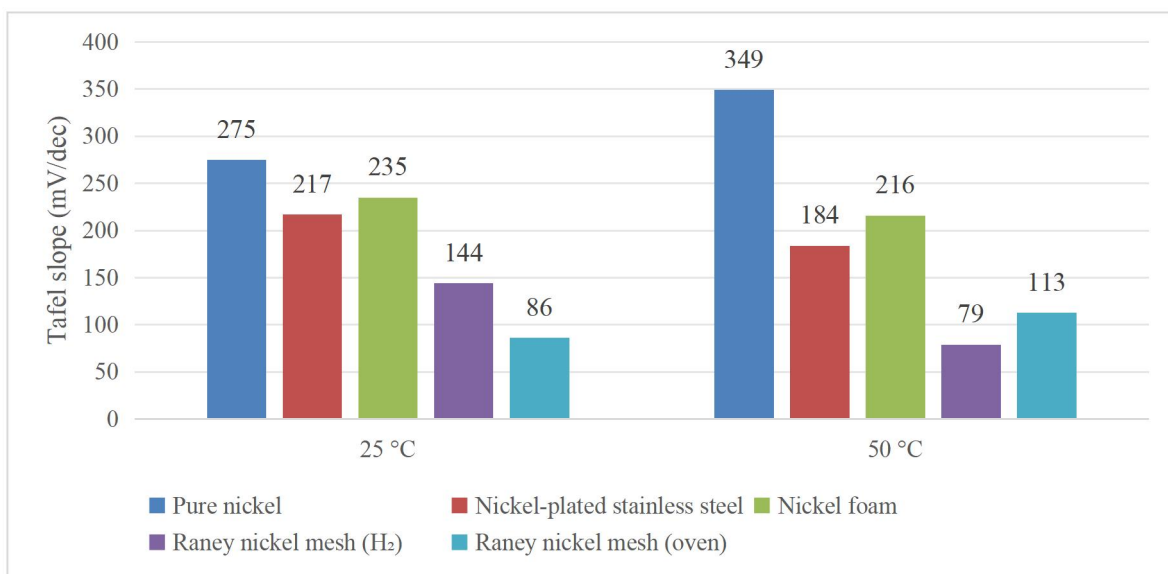


Figure 15. Tafel slopes of the cathode side.

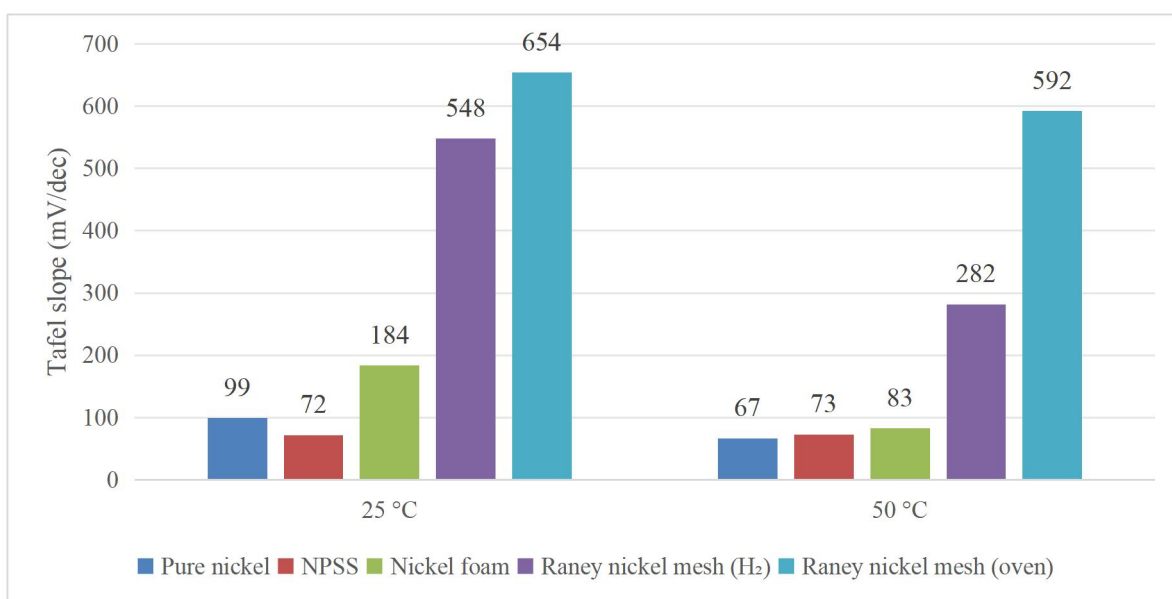


Figure 16. Tafel slopes of the anode side.

The results indicate that differences in kinetic responses are evident for all tested electrodes. Generally, porous electrodes have lower Tafel slope values than dense electrodes, suggesting better charge transfer kinetics during water electrolysis in alkaline environments. Specifically, Raney nickel exhibits the best kinetic characteristics, while nickel foam exhibits better kinetic characteristics than pure nickel and nickel-plated stainless steel. Conversely, the results for dense electrodes show higher Tafel slope values,

suggesting less favorable charge transfer kinetics and thus more kinetic limitations for water electrolysis. Moreover, it is evident that increasing the temperature from 25 °C to 50 °C improves the kinetic characteristics for all tested electrodes. This is verified by a decrease in Tafel slope values for all tested electrodes at 50 °C, suggesting better reaction kinetics and charge transfer at this temperature. Although increasing temperature improves the kinetic characteristics for all tested electrodes, the same trends for each material are evident.

The Tafel results support the trends observed for all tested electrodes in polarization and EIS measurements. Electrodes with a porous structure exhibit better electrochemical characteristics than those with a dense structure. Consequently, this Tafel analysis confirms that electrode microstructure is a key parameter for determining the catalytic characteristics for nickel-based electrodes during water electrolysis in alkaline environments.

4.4 Exchange Current Densities and Charge Transfer Coefficients

The exchange current densities and the charge transfer coefficients obtained from the Tafel plot are presented in this section to further examine the intrinsic kinetic characteristics of the investigated electrode materials. The exchange current density, j_0 , was obtained using the Tafel equation and is presented in the form of bar plots for both the cathode and the anode. Due to the significant differences in the values by several orders of magnitude, a logarithmic scale is used in the plots to better visualize the comparison of the values for the different materials.

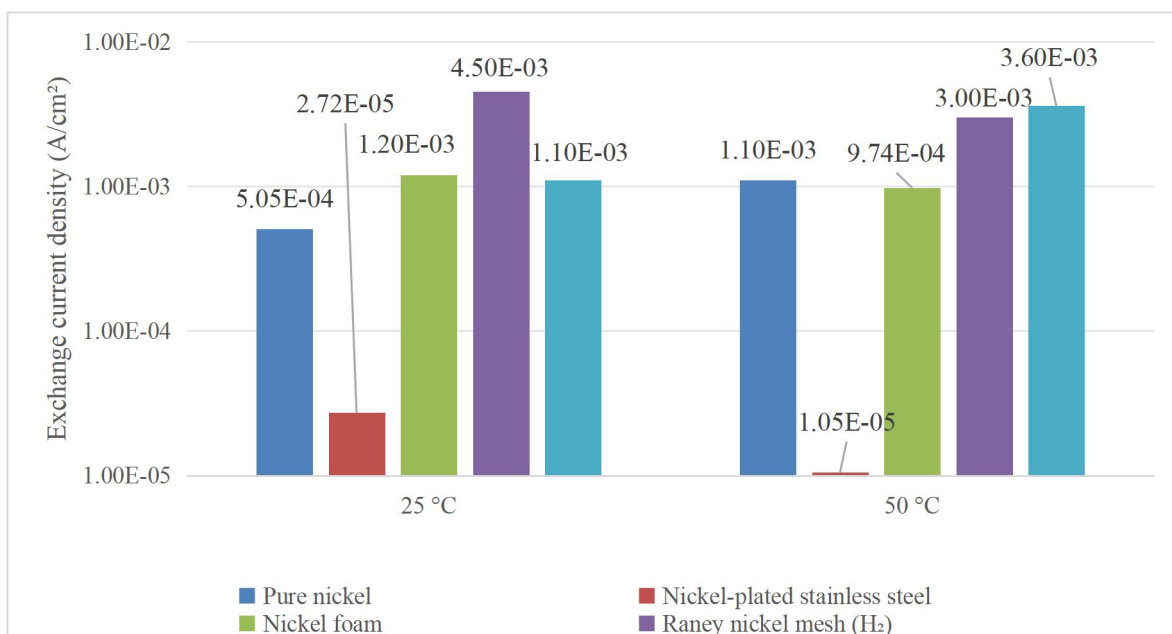


Figure 17. Exchange current densities of the cathode side.

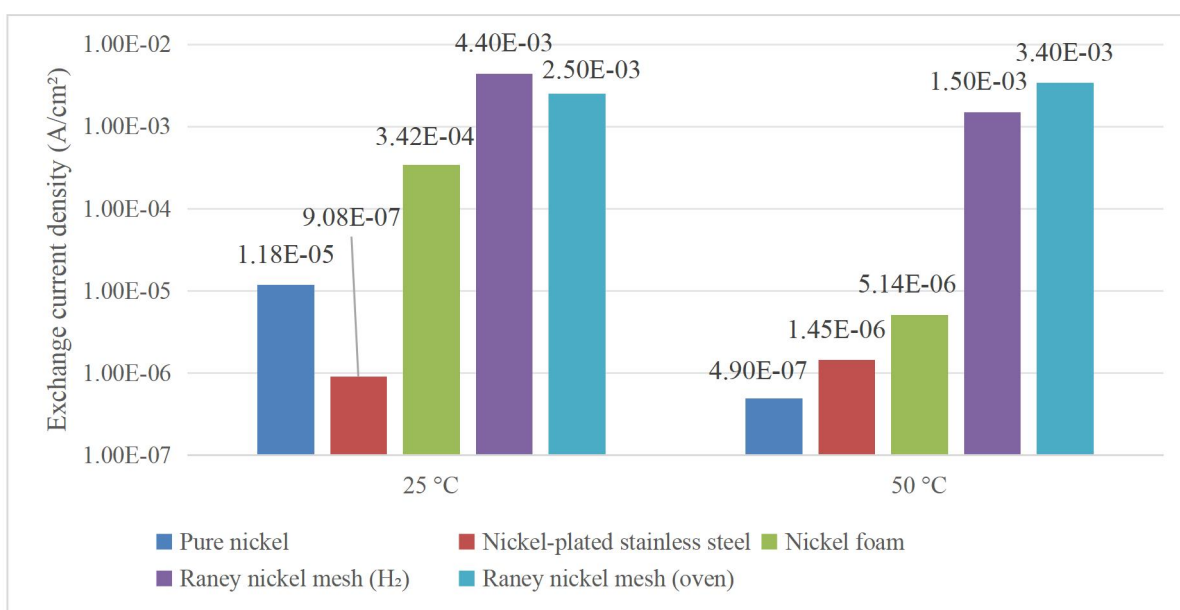


Figure 18. Exchange current densities of the anode side.

On the cathode side, nickel-plated stainless steel has the lowest exchange current density at both temperatures. This means that nickel-plated stainless steel has the least favorable cathodic kinetics. The other materials are closer to each other, and the differences are smaller for the 50 °C results. Raney nickel and nickel foam have higher exchange current

densities than the dense materials, which is consistent with the more favorable catalytic behavior observed in the polarization and Tafel curves.

On the anode side, the exchange current density for Raney nickel is significantly higher than that for the other materials, especially for the 50 °C results. In fact, the exchange current densities for the anodic reaction of Raney nickel have the same order of magnitude as those for the cathodic reaction. In contrast, for the other materials, the exchange current density for the anodic reaction is lower than that for the cathodic reaction. This means that Raney nickel has the best intrinsic activity for the anodic reaction as well. In addition, the differences in the pretreatment methods do not seem to result in significant differences in the exchange current density for Raney nickel.

The charge transfer coefficients of the cathodes and anodes are shown below as bar plots. The charge transfer coefficient, α , is inversely related to the Tafel slope. This value provides additional information about the kinetics of the electrode reaction.

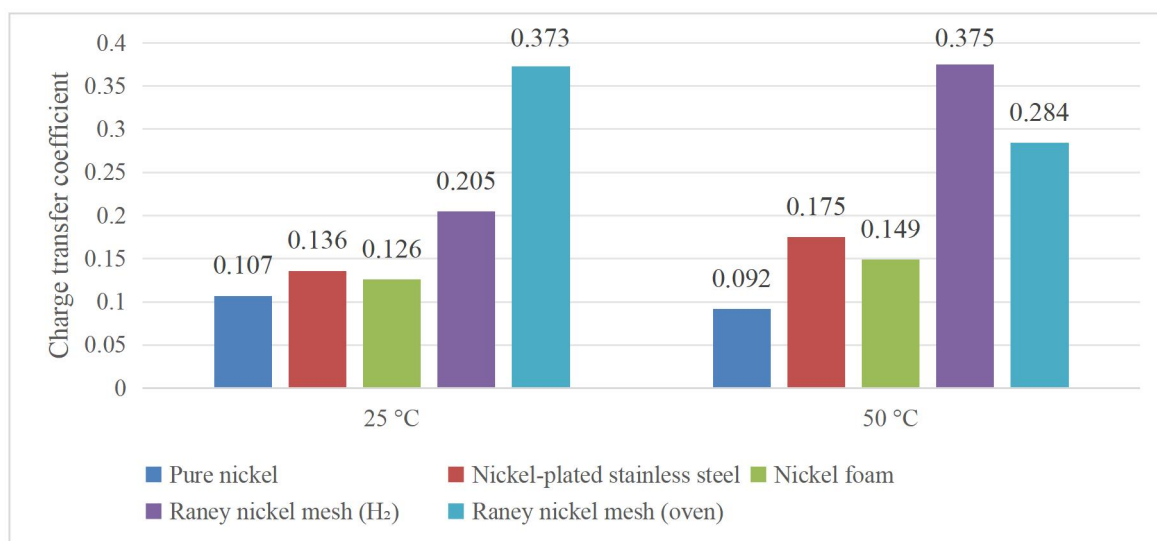


Figure 19. Charge transfer coefficients of the cathode side.

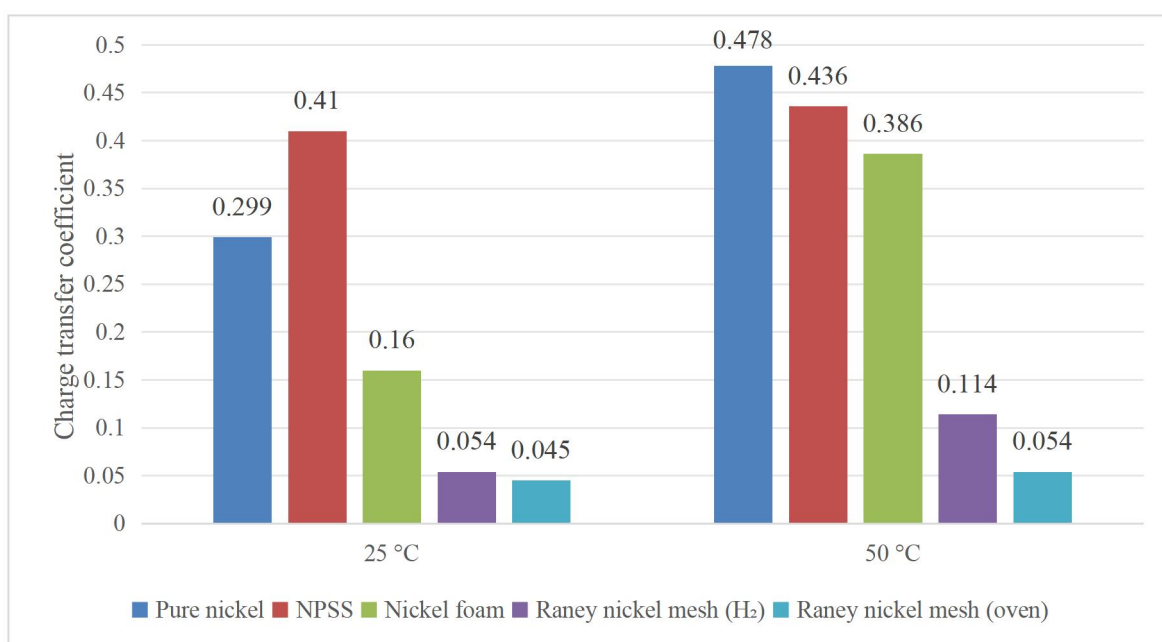


Figure 20. Charge transfer coefficients of the anode side.

For the cathodes, Raney nickel shows higher values of the charge transfer coefficients than the other materials. Depending on temperature and pretreatment, these values are clearly higher than those of nickel-plated stainless steel, pure nickel, and nickel foam. For the other materials, the coefficients are mostly within a lower range, meaning less favorable cathodic charge transfer kinetics. The temperature effect varies; the coefficients increase for some materials and decrease for others.

For the anodes, the charge transfer coefficient of Raney nickel is significantly lower than that of other materials. The charge transfer coefficient of hydrogen-activated Raney nickel anode at two temperatures is slightly higher than that of the oven pretreated Raney nickel anode. In the rest of the materials, nickel-plated stainless steel shows the highest charge transfer coefficient at 25°C, while the charge transfer coefficient of pure nickel and nickel foam increases significantly with temperature. Nevertheless, the charge transfer coefficient of all research materials at two temperatures does not reach 0.5.

In general, the results of exchange current density and charge transfer coefficient confirm that the kinetic behavior of the electrode is strongly dependent on the material structure and the reaction side. Raney nickel shows the best overall kinetic performance, including

the highest exchange current densities, while the inherent electrochemical activity of dense electrodes is relatively limited.

4.5 Comprehensive Performance Comparison and Practical Implications

From a comprehensive perspective, the overall performance level can be summarized as: Raney nickel > foam nickel > pure nickel \approx nickel-plated stainless steel. Although Raney nickel has excellent initial performance, mechanical stability, long-term durability and complexity of manufacturing process are crucial for practical applications. Nickel foam is a relatively balanced choice. It has high specific surface area, good durability and excellent mass transfer characteristics.

Therefore, the choice of electrode for alkaline electrolysis should be determined according to the needs of specific applications. High-efficiency systems may benefit from advanced porous catalysts, while large-scale industrial applications may prioritize durability, simplicity and cost-effectiveness. The results of this study provide experimental guidance for this kind of design decision-making.

Although Raney nickel exhibits the best electrochemical properties, its application should be evaluated taking into account the following factors beyond the initial activity:

- Stability and durability: Although Raney nickel exhibits high activity as a catalyst, its activity decreases over time due to sintering and leaching of the remaining aluminum elements when subjected to strong alkaline solutions. However, nickel foam exhibits high specific surface area and durability, making it a balanced and practical material choice.
- Cost and process of preparation: Nickel-plated stainless steel exhibits the best cost-effectiveness. Although pure nickel is expensive compared to nickel-plated stainless steel, its composition is easily controllable. The process of preparation of Raney nickel involves leaching steps, making the process complex and increasing the cost of preparation to some extent.
- System design factors: Raney nickel structure is relatively fragile, and specially designed electrode supports or substrates may be required in the application. The three-dimensional porous structure of nickel foam is conducive to the rapid deposition and discharge of

bubbles, and can effectively reduce the concentration overpotential under high current density.

Therefore, the choice of electrode material should be determined according to the specific application scenario. For high-end systems with high efficiency as the core goal and high-performance requirements, Raney nickel is recommended; for large-scale applications oriented by scale and cost control, paying more attention to life and system simplification, nickel foam or advanced nickel-plated structure may be a preferred solution.

5 Conclusions

The comparison of these materials was performed in alkaline water electrolysis using chronopotentiometry and electrochemical impedance spectroscopy.

The results showed that Raney nickel had the best activity among the compared materials, followed by nickel foam. However, the dense materials had higher overpotentials. These results are in accordance with the increased active surface area of porous materials, which is in agreement with the results from previous studies.

The increase in the operating temperature from 25 to 50 °C improved the activity of all materials due to the reduction in total voltage in the cell. This is because the kinetic losses are reduced. However, the relative performance ranking of the materials remained unchanged.

Even though Raney nickel showed the highest activity among the materials in this study, its long-term stability should be further evaluated. Future studies should be focused on the evaluation and optimization of the structure of nickel-based materials for their application in alkaline water electrolysis.

6 References

Bard, A.J. and Faulkner, L.R. (2001) *Electrochemical methods: fundamentals and applications*. 2nd edn. New York: Wiley. <https://dokumen.pub/electrochemical-methods-fundamentals-and-applications-3nbsped-1119334063-9781119334064.html>

Carmo, M., Fritz, D.L., Mergel, J. and Stolten, D. (2013) ‘A comprehensive review on PEM water electrolysis’, *International Journal of Hydrogen Energy*, 38(12), pp. 4901–4934. <https://www.sciencedirect.com/science/article/abs/pii/S0360319913002607>

IEA (2019) *The future of hydrogen*. Paris: International Energy Agency. <https://www.iea.org/reports/the-future-of-hydrogen>

McCrary, C.C.L., Jung, S., Peters, J.C. and Jaramillo, T.F. (2015) ‘Benchmarking heterogeneous electrocatalysts for the oxygen evolution reaction’, *Journal of the American Chemical Society*, 135(45), pp. 16977–16987. <https://pubs.acs.org/doi/10.1021/ja407115p>

O’Brien, T.F., Bommaraju, T.V. and Hine, F. (2005) *Handbook of chlor-alkali technology*. Vol. 2. New York: Springer.

Santos, A.L., Cebola, M.J., Antunes, J. and Santos, D.M.F. (2023) ‘Insights on the performance of nickel foam and stainless steel foam electrodes for alkaline water electrolysis’, *Sustainability*, 15(14), p.11011. <https://www.mdpi.com/2071-1050/15/14/11011>

Santos, D.M.F., Sequeira, C.A.C. and Figueiredo, J.L. (2013) ‘Hydrogen production by alkaline water electrolysis’, *Química Nova*, 36(8), pp. 1176–1193. <https://www.scielo.br/j/qn/a/KyQvF9DMHK6ZJXyL5zQNY7N/?lang=en>

Schalenbach, M., Zeradjanin, A.R., Kasian, O., Cherevko, S. and Mayrhofer, K.J.J. (2018) ‘A perspective on low-temperature water electrolysis – challenges and opportunities’, *Electrocatalysis*, 9(6), pp. 784–801. <https://www.sciencedirect.com/science/article/pii/S1452398123122656>

Trasatti, S. (1991) ‘Electrocatalysis by oxides—attempt at a unifying approach’, *Journal of Electroanalytical Chemistry*, 296(1–2), pp. 1–17. <https://www.sciencedirect.com/science/article/abs/pii/S0022072880800842>

Zeng, K. and Zhang, D. (2010) ‘Recent progress in alkaline water electrolysis for hydrogen production and applications’, *Progress in Energy and Combustion Science*, 36(3), pp. 307–326. <https://www.sciencedirect.com/science/article/abs/pii/S0360128509000598>

List of Figures & Tables

Figure 1. IR correction of polarization data.

Figure 2. Chronopotentiometry driver in LabVIEW.

Figure 3. Parameters for EIS measurements in the EC-Lab software.

Figure 4. Example of a Nyquist plot from an electrode EIS measurement, with the real part of the impedance on the x-axis and the imaginary part on the y-axis.

Figure 5. Tafel plots for the hydrogen evolution reaction (HER) on nickel foam electrode in alkaline water electrolysis at different temperatures. (Santos et al. 2023).

Figure 6. Anode-side resistance of different electrode materials.

Figure 7. Cathode-side resistance of different electrode materials.

Figure 8. Total cell resistances.

Figure 9. Chronopotentiometry polarization curves for pure nickel at 25 °C and 50 °C.

Figure 10. Chronopotentiometry polarization curves for nickel-plated stainless steel (NPSS) at 25 °C and 50 °C.

Figure 11. Chronopotentiometry polarization curves for nickel foam measured at 25 °C and 50 °C.

Figure 12. Chronopotentiometry polarization curves for hydrogen pre-treated Raney nickel at 25 °C and 50 °C.

Figure 13. Chronopotentiometry polarization curves for oven-treated Raney nickel at 25 °C and 50 °C.

Figure 14. One Tafel plot for pure nickel.

Figure 15. Tafel slopes of the cathode side.

Figure 16. Tafel slopes of the anode side.

Figure 17. Exchange current densities of the cathode side.

Figure 18. Exchange current densities of the anode side.

Figure 19. Charge transfer coefficients of the cathode side.

Figure 20. Charge transfer coefficients of the anode side.

Table 1. Current densities and corresponding absolute current values for the voltage measurements.